Publication title	Soot nanoparticle sizing in counterflow flames using *in-situ* particle sampling and differential mobility analysis verified with two-colour time-resolved laser-induced incandescence
Authors	Hagen, Fabian P., Vlavakis, Petros, Seitz, Malte, Klövekorn, Thomas, Bockhorn, Henning, Suntz, Rainer, Trimis, Dimosthenis
Issue Date	2022
Publisher	Elsevier
Type of publication	Journal article
Acknowledgement	The ESTiMatE project has received funding from the Clean Sky 2 Joint Undertaking under the European Union's Horizon 2020 research and innovation programme under grant agreement No 821418.
Disclaimer	The content of this article reflects only the authors' view. The Clean Sky 2 Joint Undertaking is not responsible for any use that may be made of the information it contains.

Available online at www.sciencedirect.com

ScienceDirect

Proceedings of the Combustion Institute 000 (2022) 1–10

Proceedings of the Combustion Institute

www.elsevier.com/locate/proci

SOOT

Soot nanoparticle sizing in counterflow flames using *in-situ* particle sampling and differential mobility analysis verified with two-colour time-resolved laser-induced incandescence

Fabian P. Hagen [a,b,1,*], Petros Vlavakis [a,1], Malte Seitz [a], Thomas Klövekorn [a], Henning Bockhorn [a], Rainer Suntz [b], Dimosthenis Trimis [a]

[a] *Engler-Bunte-Institute, Division of Combustion Technology, Karlsruhe Institute of Technology (KIT), Karlsruhe, Germany*
[b] *Institute for Chemical Technology and Polymer Chemistry, Karlsruhe Institute of Technology (KIT), Karlsruhe, Germany*

Received 5 January 2022; accepted 19 July 2022

Abstract

The emphasis of this work is on the development of an intrusive particle sampling system to track the evolution of soot nanoparticles in ethylene counterflow diffusion flames. The overarching objective is to determine the mobility size distributions in a spatially resolved manner using the developed probe system coupled with differential mobility analysis, i.e., a scanning mobility particle sizer (SMPS). The probe system involves a tailor-made quartz probe, gas supply, pressure control periphery, and a traverse system enabling a precise positioning along the flame axis. In preliminary experiments, the dilution ratio of the quartz probe as function of boundary conditions as well as particle losses during intrusive particle sampling are studied. To demonstrate the capability of the developed particle sampling system, results from ethylene counterflow diffusion flames with different fuel mass fractions and strain rates are presented and compared with results derived by non-intrusive laser-based diagnostics, i.e., two-colour time-resolved laser induced incandescence (2C-TiRe-LII). Results of these experiments indicate that the particle sampling system is capable of tracking the development of particle size distributions – independent of the distribution function, i.e., mono-, bi- or multimodal shape – in counterflow flames. Likewise, the agreement between soot volume fractions and particle size distributions measured via intrusive particle sampling coupled with differential mobility analysis

* Corresponding author at: Karlsruhe Institute of Technology (KIT), Engler-Bunte-Institute, Engler-Bunte-Ring 7, 76131 Karlsruhe, Germany.
E-mail address: fabian.hagen@kit.edu (F.P. Hagen).
[1] These authors contributed equally.

https://doi.org/10.1016/j.proci.2022.07.253

and non-intrusive laser-based 2C-TiRe-LII is excellent at varying the fuel mass fractions and strain rates of the ethylene counterflow flames.

Keywords: Soot nanoparticles; Intrusive particle sampling; Differential mobility analysis; Counterflow flames; Laser-induced incandescence

1. Introduction

Since soot formation bridges combustion chemistry, physics of phase transitions, fluid mechanics, heat and mass transfer, and particle dynamics, it is still one of the most complex combustion phenomena [1]. Soot formation in flames proceeds continuously from hydrocarbon fuels, soot precursor species in the gas phase to fractal aggregates of carbonaceous primary particles [1,2]. The initial steps involve the formation of soot precursor species in the gas phase and their growth to larger molecules [3]. Particle inception refers to the following transition of these gas-phase species to condensed-phased, liquid-like particles [2]. During inception, these nascent or incipient primary particles grow rapidly by coagulation and surface growth, increasing their carbon-to-hydrogen ratio and density [1,2]. As the particles evolve, they collide and form loosely bound agglomerates of the quasi-spherical primary particles with diameters d_P, which finally develop into tightly bound, chain- or grape-like fractal aggregates [2].

The transition between the phases is fluent depending on the operating conditions of the combustion process, i.e., mixture formation, flow regime, stoichiometry, temperature, residence time, and pressure [1,2]. Along with the fundamental complexity, this accounts for the many gaps in our understanding of soot formation despite decades of active research [4]. To bridge these knowledge gaps and to elucidate the underlying mechanisms of soot formation, canonical experiments were conducted in various one-dimensional model flame configurations involving well-defined boundary conditions that are decoupled from the complexity of the individual combustion system, see e.g. [4,5].

In this context, laminar counterflow flames have been used as an important highly controllable model flame configuration for soot research, enabling significant progress in understanding soot formation in recent decades [4,6-8]. A counterflow flame is quasi-one-dimensional along the normal direction of the flame, significantly facilitating the analysis of flame structures [4]. This is particularly important when validating models with detailed chemistry and particle dynamics, as computational costs are significantly reduced due to the one-dimensional nature [4,6-8]. Another major advantage of the counterflow configuration is the possibility of stabilizing premixed, partially premixed and diffusion flames [6–9].

Articles addressing soot precursor formation and particle inception in counterflow flames apply both intrusive, i.e. gas sampling coupled with chromatography and mass spectrometry (GC–MS) [6,7] and transmission electron microscopy (TEM) [10], and non-intrusive laser-based diagnostics, i.e. elastic light scattering (ELS) [9], pyrometry [8], laser extinction (LE) [11], as well as laser-induced fluorescence (LIF) [12], emission (LIE) [13] and incandescence (LII) [11,12]. While species concentration and temperature as well as soot volume fraction f_v profiles in counterflow flames are partially available [4,6-12], information is lacking on particle size distributions evolving during soot inception, coagulation, and surface growth.

An approach to determine the particle size distributions – independent of the distribution function, i.e., mono-, bi- or multimodal shape – involves particle sampling coupled with differential mobility analysis, i.e., a scanning mobility particle sizer (SMPS). Characteristics of mobility size distributions $P(d_m)$ – with the mobility diameter d_m – measured by SMPS are associated with particle inception, surface growth and coagulation rates [1,4]. According to Wang [1], these data enable the fine-tuning and validation of the soot models.

The major challenges of intrusive particle sampling in flames for mobility sizing studies are an immediate dilution of the gas sample to freeze surface growth, coagulation, and oxidation processes, while minimizing perturbation of the flame structure [4,14-16]. Addressing these requirements, Wang and co-workers developed an intrusive tubular inert gas flow-through probe system for sampling particle-laden flame gas through a small orifice [14–16]. This particle probing method has been adapted for a variety of premixed burner configurations, e.g., [14–16]. Based on the design of a gas sampling probe [17], Shariatmadar, Aleiferis, and Lindstedt recently presented a dual-port probe arrangement to sample particles in turbulent premixed flames [18]. According to Wang and Chung [4], there are still substantial challenges in developing an appropriate probe for other types of flames – especially counterflow flames – which may explain

Please cite this article as: F.P. Hagen, P. Vlavakis, M. Seitz et al., Soot nanoparticle sizing in counterflow flames using in-situ particle sampling and differential mobility analysis verified with two-colour time-resolved laser-induced incandescence, Proceedings of the Combustion Institute, https://doi.org/10.1016/j.proci.2022.07.253

why $P(d_m)$ data are not available for this model flame.

In this paper, we introduce a refined intrusive particle sampling system suitable for differential mobility analysis and enabling the *in-situ* determination of $P(d_m)$ at various heights above the fuel duct (HAFD) in counterflow flames. To demonstrate the capability of the developed particle sampling system, results from ethylene counterflow diffusion flames with different fuel mass fractions and strain rates are presented and compared with results derived by non-intrusive laser-based diagnostics, i.e., two-colour time-resolved LII (2C-TiRe-LII).

2. Methods & materials

2.1. Intrusive particle sampling system

While Section 2.1.1. presents the experimental setup and design of the sampling system, Section 2.1.2. is dedicated to the evaluation of the dilution ratio DR for calculating absolute $P(d_m)$.

2.1.1. Experimental setup & probe design

When tracking the evolution of $P(d_m)$ during soot formation using an intrusive probe method, a rapid dilution of the particle-laden gas sampled from the flame is of paramount importance to prevent changes in particle size distributions due to coagulation, diffusion, or surface reactions [4,14-16]. Consequently, a high quantity of diluent needs to be mixed immediately with the sampled flame gases, posing significant challenges to the design of an intrusive particle probe [4]. Since the dilution and sampling method presented by Wang and co-workers [14–16] is preferably applicable to premixed flames, we introduce an approach comparable to the one shown in [18] for the application in counterflow flames.

This particle sampling system consists of a dilution gas supply, the centrepiece of the system, a tailored quartz probe, and an exhaust and pressure control system of the diluted particle-laden gas sample. The assembled sampling system together with the counterflow burner and the mobility particle size analysis is shown in Fig. 1.

The dilution gas supply comprises two mass flow controllers (MFCs). Pure nitrogen is used as inert dilution gas. The primary dilution with a volume flow of $\dot{V}_{D,1}$ enters the tailored quartz probe. The second dilution step with $\dot{V}_{D,2}$ further dilutes the aerosol exiting the quartz probe.

The tailored quartz probe consists of a dilution gas inlet tube, a conical double-walled tube with an orifice at the tip to sample the particle-laden flame gas, and an outlet tube for the diluted aerosol. The probe design is similar to the dual-port arrangement developed by Lindstedt and co-workers [17,18]. The outer tube has an inner diameter of 6.0 mm and a wall thickness of 1.0 mm, whose tip narrows conically to 0.2 mm. The inner tube has an inner diameter of 3.0 mm with identical wall thickness. It is concentrically fitted into the outer tube and narrows conically to a tip diameter of 1.5 mm. The inner and outer tube form an annular chamber with an inlet for the dilution gas and the orifice at the tip. The dimensions of the two cones were chosen to minimize the distance between the tips of the inner and outer tubes to < 1.0 mm, allowing opti-

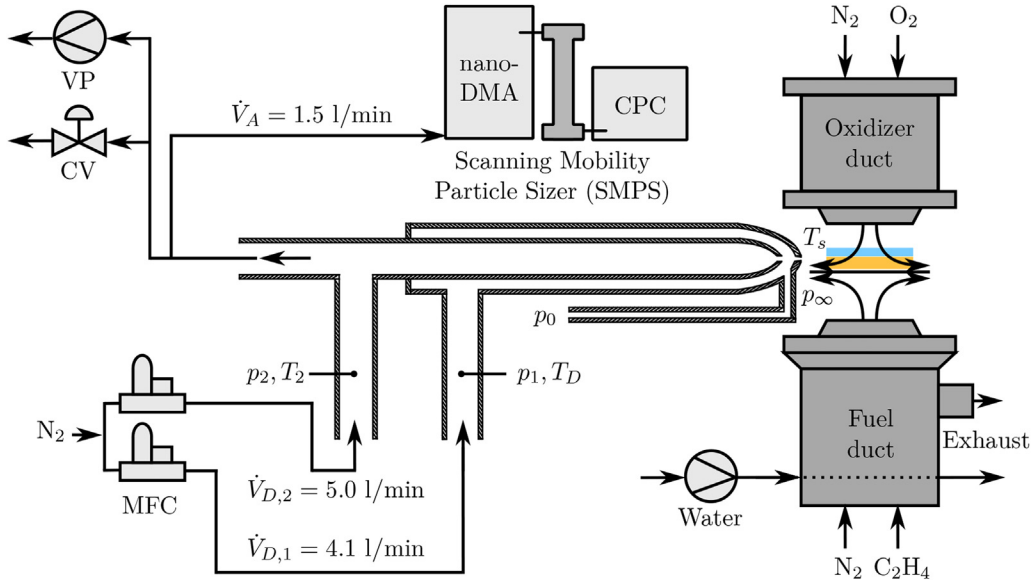

Fig. 1. Experimental setup. Not to scale.

Please cite this article as: F.P. Hagen, P. Vlavakis, M. Seitz et al., Soot nanoparticle sizing in counterflow flames using in-situ particle sampling and differential mobility analysis verified with two-colour time-resolved laser-induced incandescence, Proceedings of the Combustion Institute, https://doi.org/10.1016/j.proci.2022.07.253

mal and immediate quenching of the particle-laden flame gas. Moreover, the outer cone is intended to prevent perturbation with the counterflow flame.

A pressure gauge tube with an inner diameter of 0.8 mm is attached < 0.5 mm from the tip of the outer tube. The inlet and outlet tubes for the dilution gas and the aerosol to be analysed have an inner diameter of 3.0 mm with 1.0 mm wall thickness. Two further pressure gauge tubes are attached to the inlet and outlet tubes. Additionally, the gas temperature is measured via type K thermocouples at these positions, see Fig. 1. The probe is installed on a motor-driven traverse system enabling an exact positioning along the flame axis and sampling at different HAFD within the flame.

The diluted aerosol sample collected from the flame is drawn from the inner tube to a vacuum pump VP and the SMPS. The excess flow exiting the quartz probe passes through a control valve CV, see Fig. 1, allowing precise control of the pressure conditions, i.e., p_0, p_1 and p_2, within the system and therefore sampling rate and velocity.

For sampling, the probe tip is moved horizontally into the flame at the desired height. Based on the pressure drop $\Delta p_0 = p_\infty - p_0$, particle-laden flame gas enters the probe and is immediately quenched by the cold dilution gas nitrogen. The vacuum pump draws the diluted aerosol from the quartz probe towards the SMPS, where it is diluted with $\dot{V}_{D,2}$ in the second dilution step.

$P(d_m)$ measured via SMPS need to be corrected for particle losses. Therefore, the particle deposition in the quartz probe, the pipelines and SMPS is estimated using correlations proposed by Hinds [19] for laminar and turbulent flow regimes. Thereby, the "true" $P(d_m)$ may be calculated. The scale of corrections is 6% for $d_m > 10$ nm. For particles with $d_m < 10$ nm, the mean correction increases to ~ 45%.

Collecting a representative sample from a flame by an intrusive sampling system is challenging owing to two major difficulties, discussed in detail in e.g. [15,20,21]. First, the probe disturbs the flow and temperature field, thereby cooling the flame and affecting the gas species concentrations [15,20,21] and consequently the particle size distributions. Second, $P(d_m)$ changes due to thermophoretic deposition and reactions within the probe [14,15].

The developed quartz probe represents a compromise between rapid quenching of the extracted sample and perturbation of the flame, identified by preliminary experiments using modified probe geometries. In the final design, the tip cone and inner tube form a minimum distance ensuring an immediate quenching. As a result of this arrangement, $P(d_m)$ exhibits no systematic dependence on the dilution ratio, as discussed in the next section. Simultaneously, the flame structure is disturbed as minimally as possible by the selected cone geometry. This is confirmed by the excellent agreement of particle sizes and concentrations measured via non-intrusive 2C-TiRe-LII, see Fig. 6 and Table 1. Moreover, Shariatmadar, Hampp and Lindstedt show that a pressure drop of $\Delta p_0 <$ 2000 Pa does not induce flame perturbation [17]. Considering the working range of the introduced sampling system, see Fig. 2, a disturbance of the flame structure may be ruled out.

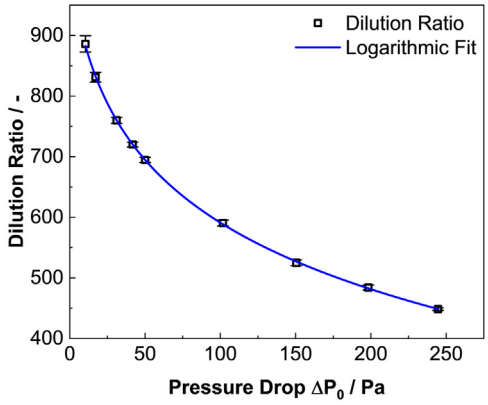

Fig. 2. Dilution ratio including the standard deviation of three repeated experiments as a function of pressure drop at the tip orifice of the probe, see Section 2.1.1. The blue curve represents a logarithmic fit to the experimental data.

2.1.2. Determination of the dilution ratio

An essential parameter for determining the absolute mobility size distributions and number densities in the flame is the dilution ratio DR. It describes the relation between the particle number density N_s measured by the SMPS and the particle number density in the flame N. This is presumed to be linear [14-16,18], hence, $N = DR \cdot N_s$ applies.

The accurate determination of DR is an essential in the development of a particle sampling system. In this study, the approach proposed by Camacho et al. is followed, measuring CO_2 concentrations of samples taken from a gas flow of pure CO_2 and/or a CO_2-diluted and stabilized premixed flame, see [16]. According to Camacho et al. [16], DR can be determined by

$$DR = \left(\frac{x_{CO_2,c}}{x_{CO_2,m}}\right)\left(\frac{T_D}{T_s}\right)\left(\frac{\mu_{m,f}}{\mu_{m,c}}\right) \quad (1)$$

from these experiments. Here, $x_{CO2,c}$ is the CO_2 mole fraction in the known calibration gas sample from the CO_2-stabilized and diluted premixed flame and/or the pure CO_2 flow. The CO_2 mole fraction of the diluted sample measured in calibration experiments is given by $x_{CO2,m}$. T_D and T_s are the temperatures of the dilution gas and sample drawn into the orifice of the tip, respectively, see Fig. 1. T_s is measured using a type K thermocouple of 150 μm diameter, which was guided through the

Please cite this article as: F.P. Hagen, P. Vlavakis, M. Seitz et al., Soot nanoparticle sizing in counterflow flames using in-situ particle sampling and differential mobility analysis verified with two-colour time-resolved laser-induced incandescence, Proceedings of the Combustion Institute, https://doi.org/10.1016/j.proci.2022.07.253

probe in the centre of the tip opening. According to [16], the mixture viscosities of the flame gas to be diluted, $\mu_{m,f}$, and the calibration gas, $\mu_{m,c}$, also need to be taken into account.

The CO_2 concentration was measured using a quadrupole mass spectrometer (QGA, Hiden Analytical). The instrument was calibrated in a concentration range between 1 ppm and 10,000 ppm. By varying the pressure drop Δp_0 at the tip orifice of the probe using the control valve CV, the dilution ratio DR can be systematically adjusted.

As proposed in [14,16], an empirical correlation of DR as a function of Δp_0 may be derived. This correlation is shown in Fig. 2 for the developed probe system and operating conditions given in Fig. 1. The correlation is obtained by fitting the experimental DRs to Δp_0 via a logarithmic function. According to the probe concept, a reduction of Δp_0 causes a decreasing intake flame gas flow rate and thus a steady increase of DR at $\dot{V}_{D,1}$ and $\dot{V}_{D,2}$=const. The studied range of DRs and Δp_0 as well as the shape of the fit are consistent with the results of [14,16,18]. Based on this correlation, DR can be determined at any given boundary condition.

The particle sampling system presented in Fig. 1 basically allows Δp_0 and thus DR to be set as desired by varying the dilution flows $\dot{V}_{D,1}$, $\dot{V}_{D,2}$ or by controlling CV. Lindstedt and co-workers found that Δp_0 and the splitting ratio between $\dot{V}_{D,1}$, $\dot{V}_{D,2}$ influence $P(d_m)$ using their dual-port probe design [18]. In preliminary studies, we therefore investigated the influence of dilution flow rates on Δp_0, DR and consequently on $P(d_m)$ for an ethylene counterflow diffusion flame with $Y_{F,1} = 0.3$ and $\alpha_2 = 60\ s^{-1}$ at HAFD = 6 mm. By varying the dilution flow rates, the range shown in Fig. 2 is extended and DRs of approx. 2000 can be realized, which simultaneously corresponds to the maximum values of [18], see also Fig. SM1 and SM2 in Supplementary Material A.

Comparable to [18], the first dilution step, i.e., the initial quenching of the flame gases, significantly impacts $P(d_m)$, while the secondary dilution has a minor effect. By exceeding a threshold value of $\dot{V}_{D,1}$ at Δp_0 = const., e.g., $\dot{V}_{D,1} \cong 3\ l{\cdot}min^{-1}$ @ $\Delta p_0 = 10$ Pa, $P(d_m)$ ceases to be a function of the primary dilution. We hypothesize that by crossing this threshold, the increased mixing velocities together with the minimum distance between the tip cone and the inner tube result in immediate quenching of the flame gases, i.e., freezing of surface growth and coagulation, rendering $P(d_m)$ invariant and thus insensitive to DR, see Supplementary Material A. In the experiments, $\dot{V}_{D,1}$ was beyond the threshold.

Since $P(d_m)$ exhibits no systematic dependence on DR, and the values shown in Fig. 2 are in agreement with [18], we chose fixed $\dot{V}_{D,1}$, $\dot{V}_{D,2}$, and Δp_0 for the experiments in this study. As noted in Fig. 1, a primary dilution flow of $\dot{V}_{D,1} = 4.1\ l{\cdot}min^{-1}$ is selected. To ensure optimal quenching of the flame gas, we selected a pressure drop at the tip orifice of the probe of $\Delta p_0 = p_\infty - p_0 = 10$ Pa, see Fig. 2. This results in a residence time of the aerosol in the probe tip before dilution of about 2 ms, which is of the order of [14] and sufficiently short to avoid particle loss. The vacuum pump draws the diluted aerosol from the probe towards the SMPS, where it is diluted with $\dot{V}_{D,2} = 5.0\ l{\cdot}min^{-1}$ in the second dilution step.

Table 1
Comparison of the CMDs from SMPS and 2C-TiRe-LII at HAFD = 5.5 mm, see Figs. 3 to 7, and peak temperatures T_{max} of the investigated flames.

$Y_{F,1}$ / -	α_2 / s^{-1}	T_{max} / K	CMD / nm	
			SMPS	2C-TiRe-LII
0.20	60	1861	3	–
0.22	60	1888	5	–
0.25	60	1928	8	10
0.30	60	1976	15	19
0.35	60	2013	23	25
0.30	70	1969	9	11
0.30	50	1984	18	25

Quantifying the accuracy of the experimentally determined dilution ratios is challenging. The measurement of the temperatures and resulting viscosities at the probe tip required in Eq. (1) are associated with uncertainties. Further, the sampling is from a volume rather than a point source, increasing the uncertainty of DR quantification. Thus, the accuracy of $P(d_m)$ and f_v is limited by the uncertainty of DR. However, the excellent agreement with the results of the non-intrusive 2C-TiRe-LII experiments, see Table 1 and Fig. 6, suggests a reasonably accurate determination of absolute $P(d_m)$ and thus DR.

2.2. Scanning mobility particle sizer

The SMPS setup, see [19,22] for theory and methodology, comprises an electrostatic classifier (EC, TSI 3938), a soft X-ray neutralizer (TSI 3088), a nano-differential mobility analyser (Nano DMA, TSI 3085A), and a condensation particle counter (CPC, TSI 3776). The EC was operated at a sheath flow rate of $15\ l{\cdot}min^{-1}$, while the CPC was operated at $\dot{V}_A = 1.5\ l{\cdot}min^{-1}$, see Fig. 1.

Since mobility sizes may overestimate d_P due to inherent limitation of the empirical Cunningham slip correction, transformation of $P(d_m)$ into $P(d_p)$ requires some scaling which is discussed in [15]. Applying the scaling shifts f_v by < 0.5% for e.g., $Y_{F,1} = 0.3$, $\alpha_2 = 4\ s^{-1}$ and HAFD = 5.5 mm, and is therefore neglected. Using the correlations proposed by Kelesidis and Pratsinis [23] accounting for fractal aggregate morphology results in an overestimation of f_v by 10% to 50%, depending on

Please cite this article as: F.P. Hagen, P. Vlavakis, M. Seitz et al., Soot nanoparticle sizing in counterflow flames using in-situ particle sampling and differential mobility analysis verified with two-colour time-resolved laser-induced incandescence, Proceedings of the Combustion Institute, https://doi.org/10.1016/j.proci.2022.07.253

the assumed primary particle size and flame condition. However, since the agreement between non-intrusive and intrusive measurements is appropriate, see Fig. 8, we did not apply their corrections. We evaluated measured $P(d_m)$ using log-normal size distributions, see e.g. [26].

2.3. Non-intrusive particle diagnostics

To validate the intrusive sampling method, an additional non-intrusive laser-based diagnostic, i.e., 2C-TiRe-LII, was applied to the investigated counterflow flames.

TiRe-LII involves heating soot particles with a nanosecond laser pulse and collecting the resulting blackbody radiation [24]. The magnitude of the incandescence signal is dependant on the soot volume fraction. Furthermore, the TiRe-LII signal decay in the low laser fluence regime provides quantitative information about the size distribution of the primary soot particles $P(d_P)$, see e.g., the review article [24] and references therein. The TiRe-LII signal decay is numerically computed with an energy balance equation for particles heated by a nanosecond laser pulse. $P(d_P)$ is determined by a multidimensional nonlinear fit of the calculated to the measured TiRe-LII signals. Approximating the size distribution by a log-normal distribution function $P(d_P)$, the first and second moments of the distribution are determined. In this study, we use the Karlsruhe model to calculate the first moment, i.e., the count median diameter (CMD), of log-normal $P(d_P)$. Comparable to Bockhorn et al. [25], we use $\sigma_g = 1.4$= const. as geometric standard deviation to ensure the best comparability of CMDs. Details, equations, and assumptions of this model are provided in [26]. The particle temperature after laser heating is determined experimentally by the two-colour method, employing Planck's radiation law. Details regarding this approach and its experimental methodology are provided in [24,26].

In the experiments, the fundamental wavelength of a 10 Hz-pulsed Nd:YAG laser at 1064 nm has been used. A rotating half-wave plate and a polarizing beam splitter are used to provide a constant and defined energy density of the laser pulses within the low-fluence regime ($f < 0.2$ J·cm^{-2}) to avoid soot particle evaporation. The TiRe-LII signal decays were collected at 120° angle to the laser beam using a lens system and two fast photomultipliers ($t_{rise} = 0.5$ ns) equipped with 10 nm FWHM band-pass interference filters centred at 450 nm and 650 nm, respectively. The laser power was continuously measured with a power-meter. Details of the two-colour detection optics, detectors, instruments, and the Nd:YAG laser used are described elsewhere [26]. A sketch of the 2C-TiRe-LII setup is provided in Fig. SM3 of Supplementary Material B.

The absolute soot volume fractions f_v were obtained by calibrating the experimental setup with a SMPS using a soot aerosol [26] from a spark discharge generator at various dilutions. Second, absolute f_v were calibrated by laser extinction using a HeNe laser at 633 nm applied to a sooty flat, acetylene premixed flame. Details of this approach are given in [27], although ethylene served as the fuel.

2.4. Counterflow burner

The experiments have been conducted in a counterflow burner configuration depicted in Fig. 1 and described in detail elsewhere [28]. The burner consists of two identical, opposed placed ducts with an inner diameter of 25 mm, and a separation distance L of 12.5 mm. The fuel mixture is added to the system through the bottom duct (1) and the oxidizer from the top (2). Both ducts are surrounded by two concentric annular ducts, where nitrogen as shielding gas is supplied. Fine wire screens with a diameter of 50 μm placed at the ducts exit ensure approximate plug-flow boundary conditions. Oxidizer, fuel, and purge gases of highest purity are supplied with MFCs. The exhaust gases are removed via a separate duct. Further details regarding the design, exhaust suction and cooling of the counterflow burner are given in [28,29].

Important operating parameters include the fuel and oxidizer mass fractions, $Y_{F,1}$, $Y_{O2,2}$, the temperature at the fuel and oxidizer boundary, T_1 and T_2, the component of the flow velocity normal to the stagnation plane at the fuel and oxidizer boundary, v_1 and v_2, and finally the strain rate α_2. In the experiments, a momentum balance $\rho_1 v_1^2 = \rho_2 v_2^2$ is imposed to keep the stagnation plane centred between the two ducts. Due to the momentum balance, the strain rate is direct correlated with v_2 and L and can be calculated from $\alpha_2 = 4 |v_2| L^{-1}$ [29].

2.5. Investigated counterflow diffusion flames

The objective of this paper is to present an intrusive sampling system for the analysis of mobility particle size distributions in counterflow flames. Therefore, the developed system was validated using counterflow flames adapted to the recommendations and target flames of the 5th international sooting flame (ISF-5) workshop [6–8]. Ethylene serves as fuel, air as oxidizer and the selected fuel mass fractions as well as the strain rates are similar to [6–8].

We investigated a total of seven ethylene/air counterflow diffusion flames near the sooting limit ($f_V < 500$ ppb) at atmospheric pressure, summarized in Table 1. The fuel mass fractions of $Y_{F,1} = 0.20, 0.22, 0.25, 0.30$ and 0.35 are varied at a constant strain rate of $\alpha_2 = 60\ s^{-1}$. To investigate the impact of the strain rate, we chose $\alpha_2 = 50\ s^{-1}$ and $70\ s^{-1}$ at $Y_{F,1} = 0.3$.

To ensure accurate operation of the counterflow burner and to evaluate $P(d_P)$ using 2C-TiRe-LII, the temperature profiles of the investigated flames

Please cite this article as: F.P. Hagen, P. Vlavakis, M. Seitz et al., Soot nanoparticle sizing in counterflow flames using in-situ particle sampling and differential mobility analysis verified with two-colour time-resolved laser-induced incandescence, Proceedings of the Combustion Institute, https://doi.org/10.1016/j.proci.2022.07.253

were determined in preliminary experiments. The experimental methodology and the results are presented in the Supplementary Material C.

3. Results & discussion

3.1. Mobility particle sizes in counterflow diffusion flames

The measured temperature profiles of the investigated flames correspond to those given in [4,6-8], see Supplementary Material C. The derived peak temperatures T_{max} listed in Table 1 and occurring at HAFD = 6.7 ± 0.1 mm also coincide with results from [6–8]. As expected, T_{max} increases with increasing fuel mass fraction and decreasing strain rate.

Particle inception in a soot formation (SF) counterflow flame starts near the flame front and the growth of the soot particles occurs toward the fuel side [4]. This is confirmed by $P(d_m)$ measured with the developed sampling system. The Figs. 3 and 4 show $P(d_m)$ as a function of HAFD for varying fuel mass fractions at a constant strain rate of $\alpha_2 = 60\ s^{-1}$. It indicates that the first particles are detected at a HAFD = 7.5 mm. Nascent particles are also formed on the fuel side, i.e., HAFD = 4.5 mm, due to the onset of particle inception.

At fuel mass fractions approaching the soot limit, i.e., $Y_{F,1} = 0.2$, $P(d_m)$ resemble monomodal

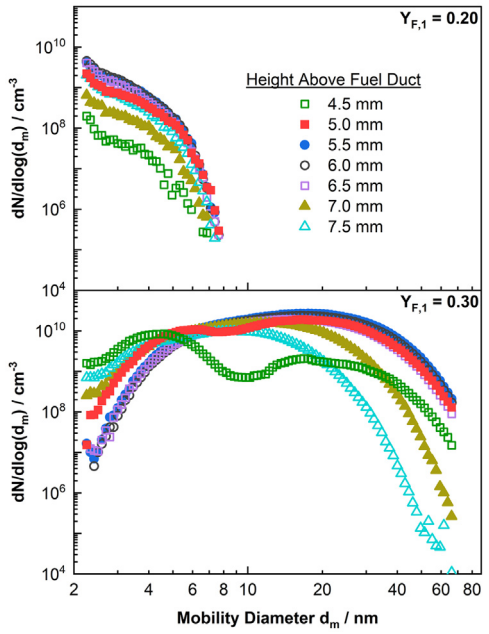

Fig. 3. $P(d_m)$ in counterflow diffusion flames with two $Y_{F,1}$ and at different HAFDs, keeping $\alpha_2 = 60\ s^{-1}$ constant.

size distributions of small nascent particles with $d_m < 8$ nm. By increasing $Y_{F,1}$, $P(d_m)$ approach log-normal distributions with a second inception mode at lower HAFD. The evolution of the distributions as function of $Y_{F,1}$ is shown in Figs. 3 and 4.

With decreasing HAFD, soot volume fractions and particle number concentrations increase sharply, reaching the maximum at HAFD = 5.5 mm, see Figs. 3–5. In contrast, the CMD of $P(d_m)$ increases only moderately, but also reaches its maximum at HAFD = 5.5 mm, see Figs. 3 and 4. Both findings are confirmed by 2C-TiRe-LII, see next section. Simultaneously, the geometric standard deviation of $\sigma_g \cong 1.55$ of the initial unimodal log-normal $P(d_m)$ at HAFD = 7.5 mm gradually increases with decreasing height, assuming a height-independent unimodal distribution, see Fig. 5.

The increase of σ_g may also be interpreted as the formation of a second inception mode while preserving the initial mode - i.e., the superposition of two narrow unimodal log-normal modes with $\sigma_g \cong 1.55$.

Figs. 3 and 4 show that an increased fuel mass fraction $Y_{F,1}$ leads to increasing soot volume fractions f_v. This may be explained by the increasing soot precursor and/or PAH concentrations with increasing $Y_{F,1}$ [4,8]In addition, the $P(d_m)$ shift to larger CMDs with increasing $Y_{F,1}$. However, particle inception outweighs surface growth and coagulation, since particle number concentrations increase from HAFD = 7.5 mm to 5.5 mm with decreasing fuel mass fraction by a factor of N(HAFD = 5.5 mm) / N(HAFD = 7.5 mm) = 3.1 ($Y_{F,1} = 0.35$) to 6.1 ($Y_{F,1} = 0.25$), while CMD(HAFD = 5.5 mm) / CMD (HAFD = 7.5 mm) increases only moderately by 1.4 ($Y_{F,1} = 0.25$) to 2.7 ($Y_{F,1} = 0.35$).

Reducing the strain rate α_2 of the counterflow diffusion flame increases its characteristic residence time $\tau \propto \alpha_2^{-1}$, thereby precursor concentration, and consequently soot formation rates [4]. Figs. 6 and 7 show the increasing soot volume fraction f_v of the three investigated strain rates of $\alpha_2 = 50\ s^{-1}$, $60\ s^{-1}$ and $70\ s^{-1}$ at $Y_{F,1} = 0.3$.

Both, the profiles as well as absolute values correspond to those reported in the literature [8,11]. The increase in f_v may be explained by the slight increase in the CMD of $P(d_m)$, which may be attributed to increased surface growth and coagulation, see Table 1. This is also shown in Fig. 5, presenting $P(d_m)$ as function of the strain rate measured at HAFD = 5.5 mm.

Mobility particle size distribution $P(d_m)$ shift similar to variation of $Y_{F,1}$ with the variation of HAFD, see Figs. 4, 7 and SM7 in Supplementary Material D. The CMD of the unimodal log-normal mobility size distribution with a geometric standard deviation of $\sigma_g \cong 1.55$ at HAFD=7.5 mm increases from approx. 10 nm to 25 nm as shown in Figs. 5, 6 and 7. Concurrently, the σ_g also increases

Please cite this article as: F.P. Hagen, P. Vlavakis, M. Seitz et al., Soot nanoparticle sizing in counterflow flames using in-situ particle sampling and differential mobility analysis verified with two-colour time-resolved laser-induced incandescence, Proceedings of the Combustion Institute, https://doi.org/10.1016/j.proci.2022.07.253

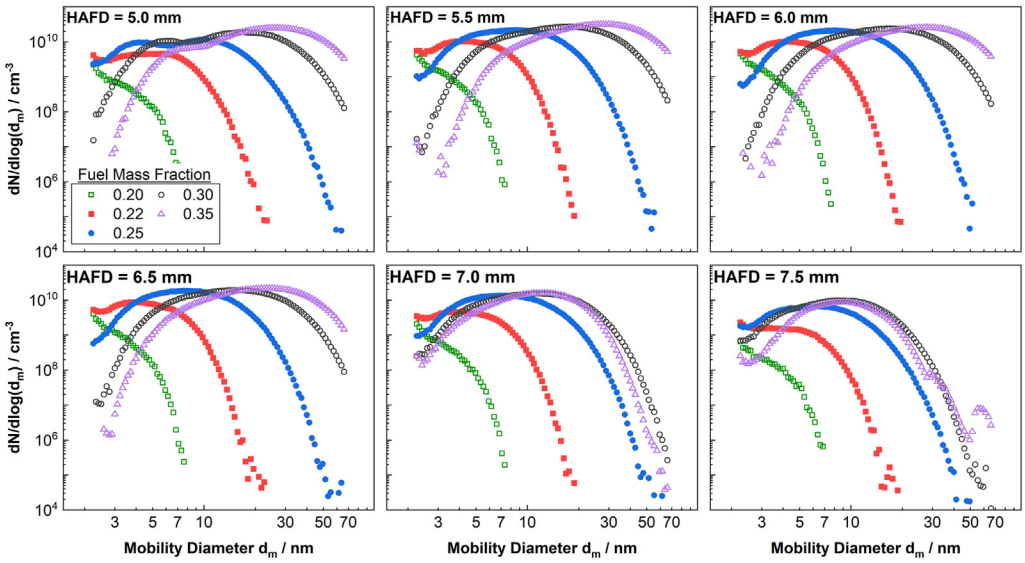

Fig. 4. $P(d_m)$ in counterflow diffusion flames with varying $Y_{F,1}$ and at different HAFDs, keeping $\alpha_2 = 60\ s^{-1}$ constant.

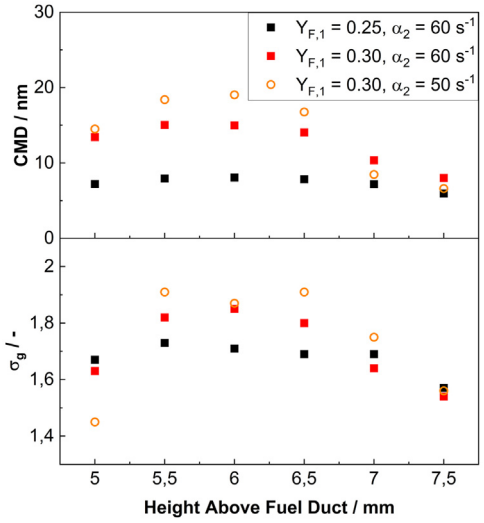

Fig. 5. Count median diameters (CMD) and geometric standard deviations of the log-normal size distributions measured via SMPS as function of HAFD.

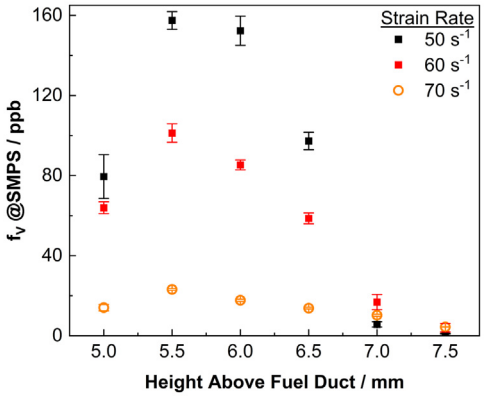

Fig. 6. Soot volume fractions f_v including the standard deviation of three repeated experiments measured via SMPS as function of HAFD for $\alpha_2 = 50\ s^{-1}$, $60\ s^{-1}$ and $70\ s^{-1}$ at $Y_{F,1} = 0.30$.

from 1.8 to 1.9, indicating the formation of a second inception mode, as discussed for the $Y_{F,1}$ variation.

3.2. Comparison of intrusive and non-intrusive particle diagnostics

Fig. 8 compares the soot volume fractions determined via the intrusive probe coupled with SMPS and non-intrusive 2C-TiRe-LII. The parity plot summarizes different counterflow flames and HAFDs as presented in Figs. 3 to 7.

Since the soot volume fractions are in excellent agreement, it may be concluded that the perturbation of the counterflow diffusion flames by the probe, see e.g. [14,15,18,20,21] is marginal. Moreover, a reasonable shift of the HAFD due to flame quenching by the probe, as discussed e.g., in [15], is not observable. The slightly reduced soot volume fractions measured by differential mobility analysis may be attributed to the limited measurement size range of 2 nm < d_m <79 nm.

Please cite this article as: F.P. Hagen, P. Vlavakis, M. Seitz et al., Soot nanoparticle sizing in counterflow flames using in-situ particle sampling and differential mobility analysis verified with two-colour time-resolved laser-induced incandescence, Proceedings of the Combustion Institute, https://doi.org/10.1016/j.proci.2022.07.253

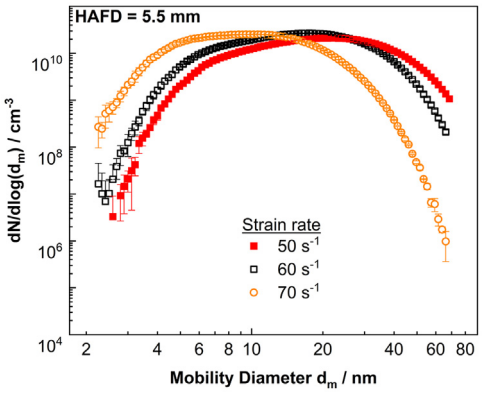

Fig. 7. $P(d_m)$ including the standard deviation of three repeated experiments at HAFD = 5.5 mm for $\alpha_2 = 50\ s^{-1}$, $60\ s^{-1}$ and $70\ s^{-1}$ and a fuel mass fraction of $Y_{F,1} = 0.30$.

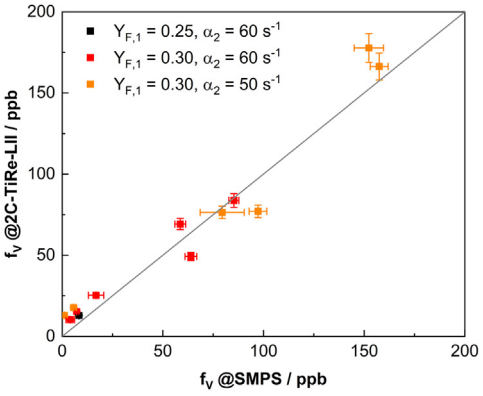

Fig 8. Comparison of the soot volume fractions from 2C-TiRe-LII and SMPS including the standard deviation of three repeated experiments.

For $Y_{F,1} = 0.20$ and 0.22 at $\alpha_2 = 60\ s^{-1}$ the signal of the 2C-TiRe-LII is below the limit of detection (LOD). $P(d_m)$ for the two flames as given in Figs. 3 and 4 suggest that the 2C-TiRe-LII signal below LOD arise rather from nascent particles being in a liquid-like state absorbing only scarcely laser light in the near-infrared (NIR) spectral region at 1064 nm [2]. However, these particles are detected by the probe coupled with SMPS revealing d_m =2 to 11 nm.

Table 1 lists the CMDs determined by SMPS and 2C-TiRe-LII for HAFD = 5.5 mm. The agreement is very good, especially considering that a) the refractive-index function for absorption to calculate the particle temperature after laser pulse heating employing Planck's radiation law is assumed to be independent of wavelength, see discussion in [26], and b) a constant value of the second moment of the log-normal size distributions has been used for 2C-TiRe-LII experiments.

4. Conclusion and final remarks

So far, particle sampling coupled with SMPS is limited to the application in premixed flames, e.g. [4,14-16,18]. In this paper, we introduced a refined particle sampling system enabling the mobility sizing in counterflow flames. The concept includes a tailor-made quartz probe, gas supply, pressure control periphery, and a traverse system. Non-intrusive 2C-TiRe-LII was used to validate the results of an initial study using ethylene counterflow diffusion flames. In validation experiments with varying HAFD, $Y_{F,1}$ and α_2, very good agreement was found between the soot volume fractions and CMDs of the particle size distributions derived from the two methods. We can even show that this combined approach may allow the resolution of the phase transition from nascent liquid-like particles to solid particles absorbing NIR light. However, a further reduction of α_2, resulting in $f_v > 500$ ppb, causes an increased particle deposition in the tip orifice. This limitation may be solved by multiple, time-reduced SMPS scans.

Declaration of Competing Interest

The authors declare that they have no known competing financial interests or personal relationships that could have appeared to influence the work reported in this paper.

Acknowledgements

The authors gratefully acknowledge the valuable discussions and ideas of Dr. Alexandra Loukou in the early stages of the probe development. This work has received funding from the Clean Sky 2 JU under European Union's Horizon 2020 research and innovation programme (G.A. No. 821418, ESTiMatE). This work was also funded by the German Research Foundation as part of TR470/7-1/2 and SU249/6-1/2.

Supplementary materials

Supplementary material associated with this article can be found, in the online version, at doi:10.1016/j.proci.2022.07.253.

References

[1] H. Wang, Formation of nascent soot and other condensed-phase materials in flames, Proc. Combust. Inst. 33 (2011) 41–67.
[2] H.A. Michelsen, M.B. Colket, P.-.E. Bengtsson, A. D'Anna, P. Desgroux, B.S. Haynes, J.H. Miller, G.J. Nathan, H. Pitsch, H. Wang, A review of terminology used to describe soot formation and evolution under combustion and pyrolytic conditions, ACS Nano 14 (2020) 12470–12490.

[3] M. Frenklach, Reaction mechanism of soot formation in flames, Phys. Chem. Chem. Phys. 4 (2002) 2028–2037.
[4] Y. Wang, S.H. Chung, Soot formation in laminar counterflow flames, Prog. Energy Combust. Sci. 74 (2019) 152–238.
[5] J.W. Martin, M. Salamanca, M. Kraft, Soot inception: carbonaceous nanoparticle formation in flames, Prog. Energy Combust. Sci. 88 (2022) 100956.
[6] L. Figura, A. Gomez, Structure of incipiently sooting ethylene–nitrogen counterflow diffusion flames at high pressures, Combust. Flame 161 (2014) 1587–1603.
[7] F. Carbone, F. Cattaneo, A. Gomez, Structure of incipiently sooting partially premixed ethylene counterflow flames, Combust. Flame 162 (2015) 4138–4148.
[8] K. Gleason, F. Carbone, A. Gomez, Effect of temperature on soot inception in highly controlled counterflow ethylene diffusion flames, Combust. Flame 192 (2018) 283–294.
[9] K. Gleason, F. Carbone, A. Gomez, PAHs controlling soot nucleation in 0.101-0.811MPa ethylene counterflow diffusion flames, Combust. Flame 227 (2021) 384–395.
[10] H.M.F. Amin, A. Bennett, W.L. Roberts, Determining fractal properties of soot aggregates and primary particle size distribution in counterflow flames up to 10 atm, Proc. Combust. Inst. 37 (2019) 1161–1168.
[11] S. Kruse, A. Wick, P. Medwell, A. Attili, J. Beeckmann, H. Pitsch, Experimental and numerical study of soot formation in counterflow diffusion flames of gasoline surrogate components, Combust. Flame 210 (2019) 159–171.
[12] B.C. Choi, S.K. Choi, S.H. Chung, Soot formation characteristics of gasoline surrogate fuels in counterflow diffusion flames, Proc. Combust. Inst. 33 (2011) 609–616.
[13] M. Sirignano, A. Collina, M. Commodo, P. Minutolo, A. D'Anna, Detection of aromatic hydrocarbons and incipient particles in an opposed-flow flame of ethylene by spectral and time-resolved laser induced emission spectroscopy, Combust. Flame 159 (2012) 1663–1669.
[14] B. Zhao, Z. Yang, J. Wang, M.V. Johnston, H. Wang, Analysis of soot nanoparticles in a laminar premixed ethylene flame by scanning mobility particle sizer, Aerosol Sci. Technol. 37 (2003) 611–620.
[15] A.D. Abid, J. Camacho, D.A. Sheen, H. Wang, Quantitative measurement of soot particle size distribution in premixed flames–the burner-stabilized stagnation flame approach, Combust. Flame 156 (2009) 1862–1870.
[16] J. Camacho, C. Liu, C. Gu, H. Lin, Z. Huang, Q. Tang, X. You, C. Saggese, Y. Li, H. Jung, L. Deng, I. Wlokas, H. Wang, Mobility size and mass of nascent soot particles in a benchmark premixed ethylene flame, Combust. Flame 162 (2015) 3810–3822.
[17] H. Shariatmadar, F. Hampp, R.P. Lindstedt, Quantification of PAH concentrations in premixed turbulent flames crossing the soot inception limit, Proc. Combust. Inst. 38 (2021) 1163–1172.
[18] H. Shariatmadar, P.G. Aleiferis, R.P. Lindstedt, Particle size distributions in turbulent premixed ethylene flames crossing the soot inception limit, Combust. Flame (2022) 111978.
[19] W.C. Hinds, Aerosol Technology. Properties, Behavior, and Measurement of Airborne Particles, John Wiley & Sons, Inc., USA, 1999.
[20] N. Hansen, T.A. Cool, P.R. Westmoreland, K. Kohse-Höinghaus, Recent contributions of flame-sampling molecular-beam mass spectrometry to a fundamental understanding of combustion chemistry, Prog. Energy Combust. Sci. 35 (2009) 168–191.
[21] Y. Karakaya, J. Sellmann, I. Wlokas, T. Kasper, Influence of the sampling probe on flame temperature, species, residence times and on the interpretation of ion signals of methane/oxygen flames in molecular beam mass spectrometry measurements, Combust. Flame 229 (2021) 111388.
[22] S.C. Wang, R.C. Flagen, Scanning electrical mobility spectrometer, Aerosol Sci. Technol. 13 (1990) 230–240.
[23] G.A. Kelesidis, S.E. Pratsinis, Determination of the volume fraction of soot accounting for its composition and morphology, Proc. Combust. Inst. 38 (2021) 1189–1196.
[24] C. Schulz, B. Kock, M. Hofmann, H. Michelsen, S. Will, B. Bougie, R. Suntz, G. Smallwood, Laser-induced incandescence: recent trends and current questions, Appl. Phys. B 83 (2006) 333.
[25] H. Bockhorn, F. Fetting, A. Heddrich, G. Wannemacher, Investigation of the formation and growth of soot particles in premixed low pressure hydrocarbon-oxygen flames, Ber. Bunsenges. Phys. Chem. 91 (1987) 819–825.
[26] F.P. Hagen, D. Kretzler, T. Häber, H. Bockhorn, R. Suntz, D. Trimis, Carbon nanostructure and reactivity of soot particles from non-intrusive methods based on UV-VIS spectroscopy and time-resolved laser-induced incandescence, Carbon N Y 182 (2021) 634–654.
[27] T. von Langenthal, M.M. Sentko, S. Schulz, B. Stelzner, D. Trimis, N. Zarzalis, Experimental characterization of flame structure and soot volume fraction of premixed kerosene jet A-1 and surrogate flames, Appl. Sci. 11 (2021) 4796.
[28] A.M. Valencia-López, F. Bustamante, A. Loukou, B. Stelzner, D. Trimis, M. Frenklach, N.A. Slavinskaya, Effect of benzene doping on soot precursors formation in non-premixed flames of producer gas (PG), Combust. Flame 207 (2019) 265–280.
[29] U. Niemann, K. Seshadri, F.A. Williams, Accuracies of laminar counterflow flame experiments, Combust. Flame 162 (2015) 1540–1549.

Please cite this article as: F.P. Hagen, P. Vlavakis, M. Seitz et al., Soot nanoparticle sizing in counterflow flames using in-situ particle sampling and differential mobility analysis verified with two-colour time-resolved laser-induced incandescence, Proceedings of the Combustion Institute, https://doi.org/10.1016/j.proci.2022.07.253